ASC *Photon.* **8**, pp. 982-987 (2021)

Title:

Terahertz-field-driven scanning tunneling luminescence spectroscopy

Author:

Kensuke Kimura[†], *Yuta Morinaga*[‡], *Hiroshi Imada*[*,†,§], *Ikufumi Katayama*[*,‡], *Kanta Asakawa*[‡], *Katsumasa Yoshioka*[‡,‖], *Yousoo Kim*[*,†], *Jun Takeda*[*,†,‡]

[†]Surface and Interface Science Laboratory, RIKEN, Wako, Japan.

[‡]Department of Physics, Graduate School of Engineering Science, Yokohama National University, Yokohama, Japan.

[§]PRESTO, Japan Science and Technology Agency (JST), Kawaguchi, Japan.

[‖]Present Address: NTT Basic Research Laboratories, NTT Corporation, Atsugi, Japan.

*Correspondence to: himada@riken.jp (H.I.), katayama-ikufumi-bm@ynu.ac.jp (I.K.), ykim@riken.jp (Y.K.), jun@ynu.ac.jp (J.T.).

Abstract:

Coupling an intense electric field of terahertz (THz) pulse to a scanning tunneling microscope (STM) has opened new avenues for conducting ultrafast electron manipulation and tracking quantum dynamics at the nanometer spatial resolution. Here we combined the THz-field-driven STM with a photon detection system and demonstrated nanospectroscopic investigations of STM-induced luminescence triggered by THz-field-driven electrons. Owing to the abundant spectral information of photons, we were able to separately measure and characterize luminescence from a localized plasmon excited by THz-field- and DC-field-driven inelastic electron tunneling. We revealed that the plasmon excitation by THz-field-driven electrons in our experiment occurred at extremely high voltage and current region due to the use of intense THz pulses, which would provide a unique experimental platform for exploring the light-matter interactions in a plasmonic nano-cavity. Our method also paves the way for investigating quantum energy dynamics accompanying quantum conversions with sub-picosecond time and atomic-scale spatial resolution.

Keywords

THz-field-driven STM, scanning tunneling luminescence, localized plasmon, inelastic tunneling, nanospectroscopy

Main text:

Electron manipulation utilizing the electric field of ultrashort laser pulses is an essential technique for revealing fundamental electron dynamics in matters and developing future high-speed electronics[1–13]. By coupling the laser pulse to an atomically sharp metal structure, the electric field is confined to the nanometer scale beyond the diffraction limit, allowing control over the electrons with extremely high spatiotemporal resolution[1–12]. Recently, a single-cycle THz electric field was installed in an STM (THz-STM)[1–9] and used to track and control carrier dynamics in matter[2,3] and molecular motions[1,4]. Although a THz-STM is capable of conducting real-time investigations of these dynamics, measurement of energy dissipations accompanying interconversions among various quanta is not yet possible because only the THz-field-driven tunneling current is measured in the method.

Photons emitted during energy dissipations provide essential information for understanding and describing energy dynamics. Scanning tunneling luminescence (STL) spectroscopy, which has developed rapidly in parallel with THz-STM spectroscopy, can measure photons converted from the tunneling electrons of an STM[14–30]. Owing to its abundant spectroscopic information on photon energy, intensity, polarization and emission efficiency, STL spectroscopy has unveiled various energy dynamics triggered by electron tunneling, such as electronic excitation and relaxation[24–28], energy conversion[18,29] and energy transfer[30], in quantum systems with nanometer spatial resolution.

Here, we report the development of THz-field-driven STL (THz-STL) spectroscopy by combining the THz-STM and STL techniques to capture the energy dynamics triggered by ultrafast electron tunneling (Fig. 1a). THz pulses were guided into a low-temperature STM and focused onto the tip by using a lens placed on the STM stage. Photons induced by the THz transients were collected using another lens and directed to a photon detector (see Methods section). We measured visible photon emission from the radiative decay of the collective oscillation of electrons (plasmon)[14–22,26,27] as a demonstration of nanospectroscopic investigation on energy dynamics by THz-STL spectroscopy.

A single-cycle THz pulse with a maximum electric field of 188 V/cm (Fig. 1b) was focused onto a Au tip to drive electrons in the STM junction (Fig. S1). Figure 1c shows a current trace recorded on Ag(111), where the current induced by THz pulses (I_{THz}) was measured as 2.65 pA. Since the repetition rate of the laser was 100 kHz, a single THz pulse drove ~165 net electrons in the case shown in Fig. 1c. According to the simulation based on the Simmons model[2,5,6,10,31], for the electron tunneling probability, the maximum magnitude of the voltage applied by the THz pulse (V_{THz}) was estimated to be ~6.5 V (Fig. S2).

Figure 1d shows luminescence spectra when the THz pulse was either introduced to the STM (red spectrum) or blocked (grey spectrum). Whereas no peak is evident in the grey spectrum, a broad peak ranging from 1.3 eV to 2.3 eV appears in the red spectrum, indicating that the peak was due to the THz pulses.

Figures 2a and 2b show a series of THz-STL spectra and current traces at different THz intensities. When the THz intensity was the highest ($\theta = 0°$), the magnitudes of the THz-STL and I_{THz} signals were the largest and the intensities decreased with decreasing THz intensities. Figure 2c shows the I_{THz} dependence of luminescence intensity. The luminescence intensity was increased as the I_{THz} was increased, which clearly shows that the observed luminescence was triggered by the THz transients.

It is well known that a broad peak in a steady-state STL spectrum of a metallic tip-sample junction originates from the radiative decay of a plasmon localized in the gap[14–22,26,27], which is excited by inelastic tunneling (IET). Since the resonance shape of the localized plasmon can be tuned by modifying the tip condition[18,26,27], we prepared three different tip conditions and measured THz-STL and steady-state STL spectra to confirm the origin of the broad peak in the THz-STL spectra (Fig. 2d). The shapes of the THz-STL spectra were identical to those of the corresponding steady-state STL spectra, indicating that the broad peak originated from a localized plasmon excited by the THz-field-

driven electrons. Thus, we concluded that THz-field-driven IET accompanying plasmon excitation occurred during the THz-STL measurements.

To elucidate the mechanistic differences of plasmon excitations by the static and pulsed electric fields, we compared the plasmon excitations by DC-field-driven and THz-field-driven electrons in THz-STL and STL measurements. The grey spectrum in Fig. 3a is an STL spectrum obtained with the feedback loop turned off with DC sample voltage (V_{DC}) of 1.9 V and tunnel current (I_{DC}) of 10 pA. A broad peak due to luminescence from a localized plasmon was observed with a quantum cut-off at 1.9 eV determined by V_{DC} = 1.9 V. When the THz pulse was irradiated, the total current increased to 13 pA (inset, Fig. 3a) and the luminescence intensity in the THz-STL spectrum (shown in blue in Fig. 3a) was slightly increased below 1.9 eV and additional luminescence was observed above 1.9 eV.

Next, we changed V_{DC} from 1.5 to 2.0 V and measured THz-STL and STL spectra (Fig. 3b). The cut-off energies of plasmon were shifted depending on V_{DC} in the STL spectra. In all the THz-STL spectra, luminescence induced by THz transients was observed above the cut-off energies and the luminescence intensities were slightly increased below the cut-off energies. To extract the luminescence component due to the THz transients, we subtracted the STL spectra from the THz-STL spectra (Fig. 3c) and found that the luminescence components were almost identical for all the THz-STL spectra with different V_{DC}. These results indicate that the V_{THz}, which reached 6.5 V at maximum, excites a plasmon regardless of V_{DC}.

These results also show that the luminescence peak originating from the DC electron tunneling was not affected by the presence or absence of THz pulses. The independence of plasmon excitation by I_{THz} and I_{DC} can be rationalized by considering how these currents flow. As shown in Fig. 1c, ~165 net electrons were driven by a THz pulse with 100 kHz repetition. In contrast, when I_{DC} = 10 pA, the average time interval between DC electron tunneling events was 16 ns, corresponding to an average

repetition rate of 62 MHz. Owing to this mismatch of repetition rates, the plasmon excitation by THz-field-driven IET was independent of DC-driven IET.

To further investigate the THz-field-driven IET, we examined the luminescence efficiency of the localized plasmon. As shown by the spectral features below 1.9 eV in the THz-STL and STL spectra (Fig. 3a), the luminescence efficiency of the localized plasmon by I_{THz} was smaller than that of I_{DC}, which is precisely confirmed in Fig. S3. This is because the plasmon luminescence efficiency varies within the picosecond timescale owing to the time evolution of V_{THz} ($V_{THz}(t)$; Fig. 3d). Since the magnitude of $V_{THz}(t)$ reached a maximum of ~6.5 V, elastic tunneling (ET) and IET via a field emission resonance (FER) should be taken into account in our THz-STL experiments (Figs. S4 and S5). When ET to a FER is the dominant tunneling process (Fig. 3d(ii)), the luminescence efficiency of a localized plasmon is small because ET cannot contribute to its excitation (as experimentally confirmed by steady-state STL measurements in Fig. S5 and previous reports[15,19]). In contrast, when a higher voltage is applied to the STM junction (Fig. 3d(iii)), IET pathways via the FER are opened and the localized plasmon starts to be excited, increasing the luminescence efficiency. The luminescence efficiency during THz-STL measurement varies within the picosecond timescale owing to the changes in $V_{THz}(t)$ but is constant during steady-state STL measurement. Note that the peak top of THz pulse (Fig. 3d(iii)) mainly contributes to the plasmon excitation, owing to the highly nonlinear *I*-*V* curve at high voltage regions. According to the simulation in Fig. S2c, the most of tunneling electrons flow at the moment when V_{THz} reaches ~6.5 V (I = ~250 μA), where the luminescence efficiency per tunneling electron may be small compared to the lower voltages in tunnel region. Since many electrons are confined in time at V_{THz} = ~6.5 V, there is also a possibility that the correlation between the tunneling electrons may affect the efficiency in our experiment[22]. It should be noted that the THz-STL spectroscopy is capable of characterizing the plasmon excited at this extreme voltage and current condition, which is not accessible by the steady-state STL spectroscopy. Furthermore, we anticipate that this unique

plasmon source would open the door for novel plasmon-induced chemical reactions under high electric field[32,33].

Finally, to examine the spatial resolution in THz-STL spectroscopy, we deposited metal atoms onto a Ag(111) surface to fabricate a nanostructure with a different work function[34] and conducted THz-STL measurements. Figure 4a shows an STM image of a Au-island grown on Ag(111). The Au-island had a herringbone structure, which is a well-known reconstruction structure on a Au(111) surface[10]. The height of the Au-island was smaller than an atomic step of Ag(111), indicating that the Au forms one atomic reconstructed layer on Ag(111). Figure 4b shows THz-STL spectra with the tip located over a Au-island or Ag(111). The luminescence efficiency was clearly higher in the case of the Au-island. To demonstrate the nanoscopic capability of the method, we compared the luminescence efficiency between the Au-island and Ag(111) surface by acquiring THz-STL spectra along the line shown in Fig. 4a. A difference in luminescence intensity was detected at the boundary between the Au-island and Ag(111) (Fig. 4c), confirming the nanometer spatial resolution of THz-STL spectroscopy.

In conclusion, we demonstrated the potential of THz-STL spectroscopy for investigating energy dynamics triggered by THz transients. Owing to the abundant spectral information, we clarified the properties of plasmon excitation triggered by the intense THz single-cycle pulse. The use of intense THz-field instead of DC-field offers a novel opportunity to utilize a plasmonic nano-cavity at extreme conditions and investigate light-matter interactions in the cavity, such as Raman scattering[35–37], field-induced phase transition[38], and chemical reaction[32]. Furthermore, by monitoring the photon intensity as a function of time after THz pulse irradiation, various energy dynamics triggered by electron tunneling in matters including semiconductors[2,3,24,25] and molecular systems[1,4,18,26–30] can be measured with the sub-nanometer spatial resolution of an SMT. We anticipate that this real-time and real-space spectroscopy offers prospects for sensing and controlling quantum systems, providing novel insights and advances in nanoscale science and technology.

Methods

Methods and associated references are available in the Supporting Information.

Associated Content

Supporting Information

This material is available free of charge via the internet at ****

Method, simulation of THz-field-driven tunnel current, discussion of efficiency difference between THz-STL and STL measurements, and investigation of plasmon luminescence property at a field emission region (PDF)

Author Contributions

K.K., H.I., I.K., and K.Y. designed the experiments. Y.M., I.K., K.A., K.Y., and J.T. designed and built the THz generation system. K.K., H.I., and Y.K. upgraded the STM for THz experiments. K.K., Y.M., and K.A. performed the experiments. K.K., H.I. and I.K. analyzed the data and conducted the simulation. Y.K. and J.T. directed the project. All authors discussed the results and wrote the manuscript.

Competing interests

The authors declare no competing financial interest.

Author Information

Correspondence and requests for materials should be addressed to H.I. (himada@riken.jp), I.K. (katayama-ikufumi-bm@ynu.ac.jp), Y.K. (ykim@riken.jp) or J.T. (jun@ynu.ac.jp).

Acknowledgements

This work was financially supported by KAKENHI (Grant No. 20H05662, 20H00326, 18H05257, 17H06124, 20H02653, 17H04796, 18J11856, 20K22488) and JST PRESTO (Grant No. JPMJPR1862) of the Ministry of Education, Culture, Sports, Science, and Technology (MEXT) of Japan. K.K. acknowledges the Special Postdoctoral (SPDR) program of RIKEN and MEXT/JSPS Fellowship (18J11856). We acknowledge Prof. Koichiro Tanaka at Kyoto University for his help with constructing the experimental setup. We thank M. Horikawa, N. Hayazawa, R. B. Jaculbia, Y. Arashida, M. Balgos, M. Imai-Imada, K. Miwa, and J. Takeya for helpful discussions. In addition, we thank Y. Hasegawa and Y. Shimizu for supporting preparation of the STM tip.

Data availability

All data that support the findings of this study are available from the corresponding authors upon reasonable request.

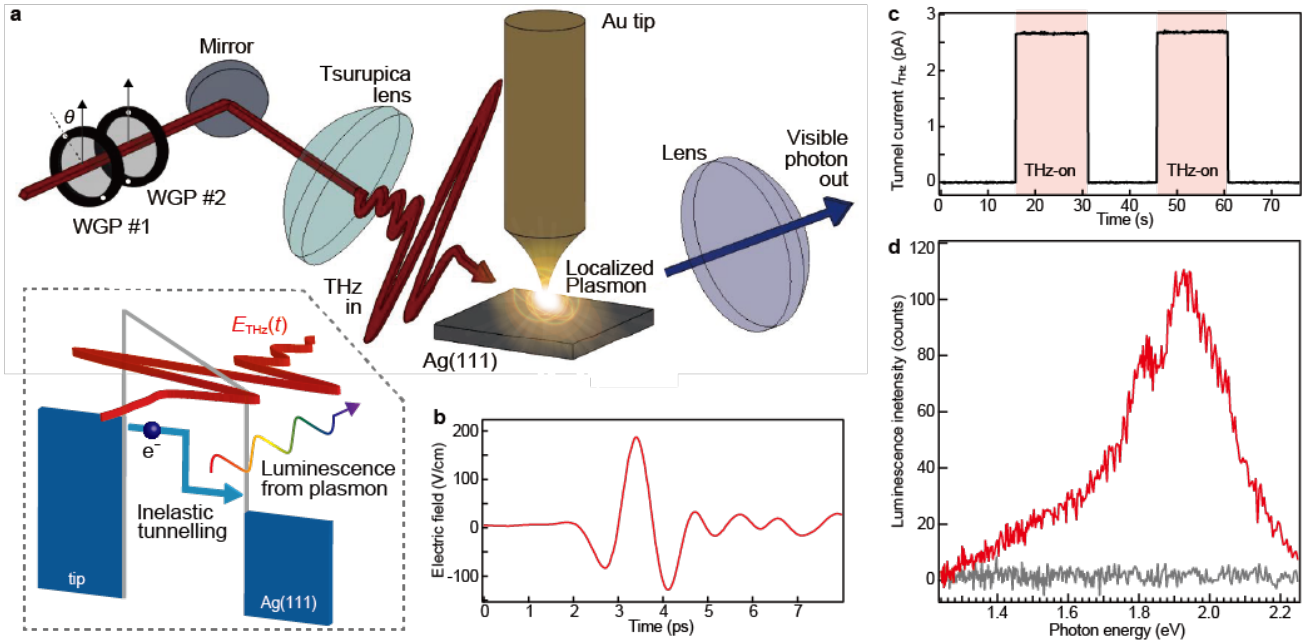

Figure 1. (a) Schematic of THz-STL measurement. The intensity of the THz electric field is adjustable by changing the relative angle (θ) of wire grid polarizers (WGPs). The inset shows the basic concept. Luminescence from a localized plasmon is induced by THz-field-driven inelastically tunneled electrons. (b) Temporal profile of a single-cycle THz electric field measured using electro-optical sampling. (c) Current trace with and without THz pulses. The feedback loop was turned off when the DC sample voltage (V_{DC}) was 1.0 V and tunnel current (I_{DC}) was 10 pA, then V_{DC} was changed to 0 V, leading I_{DC} = 0 pA. (d) THz-STL spectra of Ag(111) (V_{DC} = 0 V, exposure time t = 120 s) with (red spectrum) and without (grey spectrum) THz.

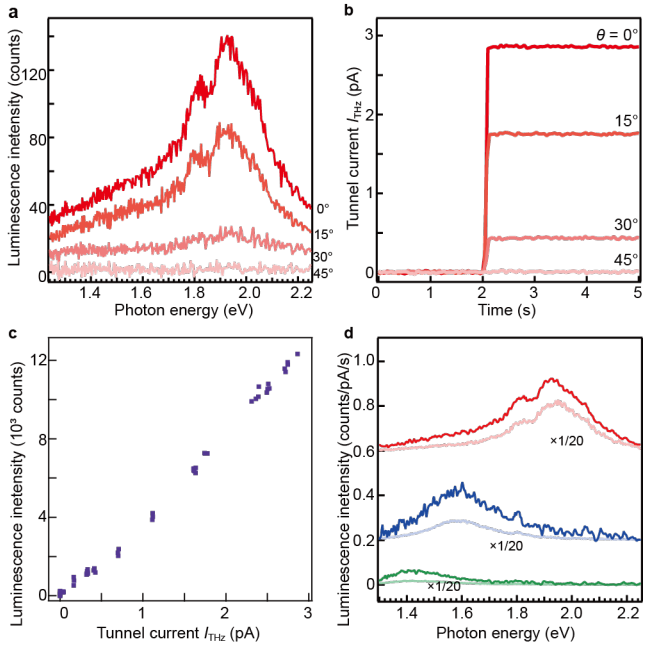

Figure 2. (a) THz intensity dependence of THz-STL spectra (V_{DC} = 0 V, t = 120 sec). The intensity of the THz electric field was changed by using two wire grid polarizers (WGPs) as shown in Fig. 1(a). WGP#2 was fixed to introduce parallel-polarized THz pulses to the tip-sample direction, and the angle of WGP#1 with respect to WGP#2 (θ) was changed from 0° to 45°. The spectrum at 0° is identical to the one in Fig. 1d. (b) THz intensity dependence of current traces. (c) I_{THz} dependence of luminescence intensity (V_{DC} = 0 V, t = 120 sec). (d) THz-STL and STL spectra obtained with three different tip conditions. Darker colors denote THz-STL spectra (V_{DC} = 0 V) and lighter colors STL spectra (V_{DC} = 2.5 V). The dark red spectrum is identical to the one in Fig. 1d.

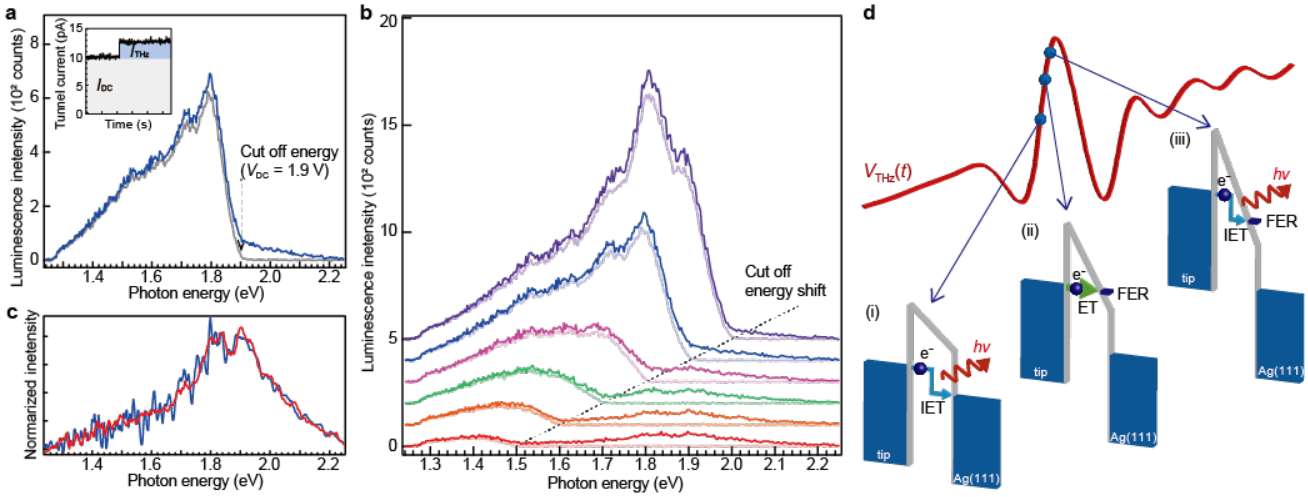

Figure 3. (a) THz-STL (blue) and STL (grey) spectra at V_{DC} = 1.9 V (t = 120 s). During luminescence measurements, the feedback loop was turned off at V_{DC} = 1.9 V and I_{DC} = 10 pA. Inset shows the current trace at V_{DC} = 1.9 V with I_{DC} and I_{THz} components distinguished by grey and blue rectangles, respectively. The cut-off energy is shown as an arrow. (b) Series of THz-STL (darker color) and STL (lighter color) spectra at different V_{DC} ($1.5 < V_{DC} < 2.0$ V, I_{DC} = 10 pA, t = 120 s): purple 2.0 V, blue 1.9 V (identical to spectra in Fig. 3(a)), pink 1.8 V, green 1.7 V, orange 1.6 V, red 1.5 V. The shift in cut-off energy in STL spectra is indicated by a dotted line. (c) Subtraction of THz-STL from STL spectra in b (blue; 1.9 V, red; 1.5 V). (d) Schematic of plasmon excitation mechanisms. V_{THz} varied within the picosecond timescale (red line). Depending on the time evolution of the voltage, the energy diagram at the STM junction changed according to (i)-(iii): (i) shows the IET process (sky-blue arrow) at the tunneling region, (ii) shows energy diagram when the ET process to the FER (green arrow) is more dominant than the IET accompanying plasmon excitation, (iii) shows the IET process via the FER.

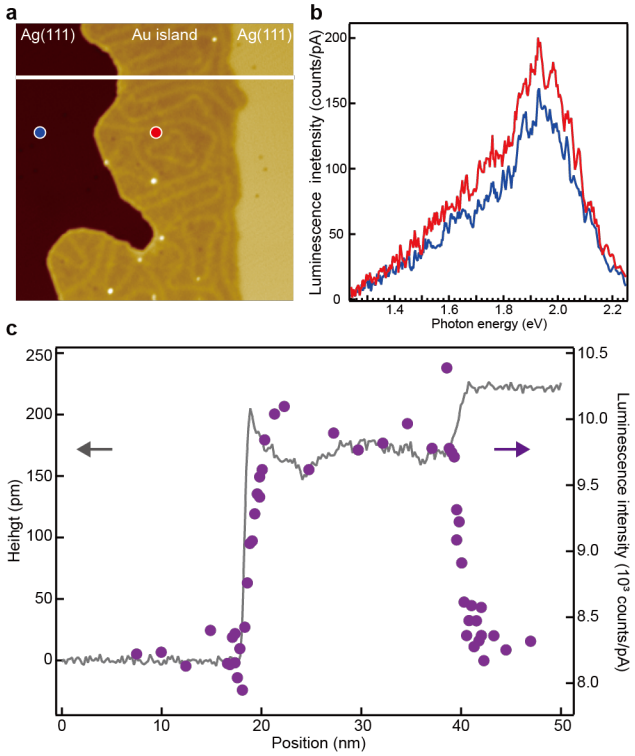

Figure 4. (a) STM image of Au-island/Ag(111) (50 × 50 nm^2, V_{DC} = 1.0 V, I_{DC} = 10 pA). (b) THz-STL spectra of Au-island (red spectrum) and Ag(111) (blue spectrum) obtained at V_{DC} = 0 V and t = 120 s. The THz-STL spectra of the Au-island and Ag(111) were measured with the tip located at red and blue points in Fig. 4(a), respectively. (c) Height profile and photon efficiency profile along the white line in Fig. 4(a). THz-STL spectra were measured at V_{DC} = 0 V and t = 120 s.

References

(1) Peller, D.; Kastner, L. Z.; Buchner, T.; Roelcke, C.; Albrecht, F.; Moll, N.; Huber, R.; Repp, J. Sub-Cycle Atomic-Scale Forces Coherently Control a Single-Molecule Switch. *Nature* **2020**, *585* (7823), 58–62. https://doi.org/10.1038/s41586-020-2620-2.

(2) Cocker, T. L.; Jelic, V.; Gupta, M.; Molesky, S. J.; Burgess, J. A. J.; Reyes, G. D. L.; Titova, L. V.; Tsui, Y. Y.; Freeman, M. R.; Hegmann, F. A. An Ultrafast Terahertz Scanning Tunnelling Microscope. *Nat. Photonics* **2013**, *7* (8), 620–625. https://doi.org/10.1038/nphoton.2013.151.

(3) Jelic, V.; Iwaszczuk, K.; Nguyen, P. H.; Rathje, C.; Hornig, G. J.; Sharum, H. M.; Hoffman, J. R.; Freeman, M. R.; Hegmann, F. A. Ultrafast Terahertz Control of Extreme Tunnel Currents through Single Atoms on a Silicon Surface. *Nat. Phys.* **2017**, *13*, 591–598. https://doi.org/10.1038/nphys4047.

(4) Cocker, T. L.; Peller, D.; Yu, P.; Repp, J.; Huber, R. Tracking the Ultrafast Motion of a Single Molecule by Femtosecond Orbital Imaging. *Nature* **2016**, *539* (7628), 263–267. https://doi.org/10.1038/nature19816.

(5) Yoshioka, K.; Katayama, I.; Minami, Y.; Kitajima, M.; Yoshida, S.; Shigekawa, H.; Takeda, J. Real-Space Coherent Manipulation of Electrons in a Single Tunnel Junction by Single-Cycle Terahertz Electric Fields. *Nat. Photonics* **2016**, *10* (12), 762–765. https://doi.org/10.1038/nphoton.2016.205.

(6) Yoshioka, K.; Katayama, I.; Arashida, Y.; Ban, A.; Kawada, Y.; Konishi, K.; Takahashi, H.; Takeda, J. Tailoring Single-Cycle Near Field in a Tunnel Junction with Carrier-Envelope Phase-Controlled Terahertz Electric Fields. *Nano Lett.* **2018**, *18* (8), 5198–5204. https://doi.org/10.1021/acs.nanolett.8b02161.

(7) Yoshida, S.; Hirori, H.; Tachizaki, T.; Yoshioka, K.; Arashida, Y.; Wang, Z.-H.; Sanari, Y.; Takeuchi, O.; Kanemitsu, Y.; Shigekawa, H. Subcycle Transient Scanning Tunneling Spectroscopy with Visualization of Enhanced Terahertz Near Field. *ACS Photonics* **2019**, *6* (6), 1356–1364. https://doi.org/10.1021/acsphotonics.9b00266.

(8) Müller, M.; Martín Sabanés, N.; Kampfrath, T.; Wolf, M. Phase-Resolved Detection of Ultrabroadband THz Pulses inside a Scanning Tunneling Microscope Junction. *ACS Photonics* **2020**, *7* (8), 2046–2055. https://doi.org/10.1021/acsphotonics.0c00386.

(9) Luo, Y.; Jelic, V.; Chen, G.; Nguyen, P. H.; Liu, Y.-J. R.; Calzada, J. A. M.; Mildenberger, D. J.; Hegmann, F. A. Nanoscale Terahertz STM Imaging of a Metal Surface. *Phys. Rev. B* **2020**, *102* (20), 205417. https://doi.org/10.1103/PhysRevB.102.205417.

(10) Garg, M.; Kern, K. Attosecond Coherent Manipulation of Electrons in Tunneling Microscopy. *Science* **2020**, *367* (6476), 411–415. https://doi.org/10.1126/science.aaz1098.

(11) Ludwig, M.; Aguirregabiria, G.; Ritzkowsky, F.; Rybka, T.; Marinica, D. C.; Aizpurua, J.; Borisov, A. G.; Leitenstorfer, A.; Brida, D. Sub-Femtosecond Electron Transport in a Nanoscale Gap. *Nat. Phys.* **2020**, *16* (3), 341–345. https://doi.org/10.1038/s41567-019-0745-8.

(12) Du, S.; Yoshida, K.; Zhang, Y.; Hamada, I.; Hirakawa, K. Terahertz Dynamics of Electron–Vibron Coupling in Single Molecules with Tunable Electrostatic Potential. *Nat. Photonics* **2018**, *12* (10), 608–612. https://doi.org/10.1038/s41566-018-0241-1.

(13) Schiffrin, A.; Paasch-Colberg, T.; Karpowicz, N.; Apalkov, V.; Gerster, D.; Mühlbrandt, S.; Korbman, M.; Reichert, J.; Schultze, M.; Holzner, S.; Barth, J. V.; Kienberger, R.; Ernstorfer, R.; Yakovlev, V. S.; Stockman, M. I.; Krausz, F. Optical-Field-Induced Current in Dielectrics. *Nature* **2013**, *493* (7430), 70–74. https://doi.org/10.1038/nature11567.

(14) Berndt, R.; Gimzewski, J.; Johansson, P. Inelastic Tunneling Excitation of Tip-Induced Plasmon Modes on Noble-Metal Surfaces. *Phys. Rev. Lett.* **1991**, *67* (27), 3796–3799. https://doi.org/10.1103/PhysRevLett.67.3796.

(15) Berndt, R.; Gimzewski, J. K. Isochromat Spectroscopy of Photons Emitted from Metal Surfaces in an STM. *Ann. Phys.* **1993**, *505* (2), 133–140. https://doi.org/10.1002/andp.19935050205.

(16) Liu, S.; Wolf, M.; Kumagai, T. Plasmon-Assisted Resonant Electron Tunneling in a Scanning Tunneling Microscope Junction. *Phys. Rev. Lett.* **2018**, *121* (22), 226802. https://doi.org/10.1103/PhysRevLett.121.226802.

(17) Böckmann, H.; Liu, S.; Müller, M.; Hammud, A.; Wolf, M.; Kumagai, T. Near-Field Manipulation in a Scanning Tunneling Microscope Junction with Plasmonic Fabry-Pérot Tips. *Nano Lett.* **2019**, *19* (6), 3597–3602. https://doi.org/10.1021/acs.nanolett.9b00558.

(18) Imada, H.; Miwa, K.; Imai-Imada, M.; Kawahara, S.; Kimura, K.; Kim, Y. Single-Molecule Investigation of Energy Dynamics in a Coupled Plasmon-Exciton System. *Phys. Rev. Lett.* **2017**, *119* (1), 013901. https://doi.org/10.1103/PhysRevLett.119.013901.

(19) Martínez-Blanco, J.; Fölsch, S. Light Emission from Ag(111) Driven by Inelastic Tunneling in the Field Emission Regime. *J. Phys. Condens. Matter* **2015**, *27* (25), 255008. https://doi.org/10.1088/0953-8984/27/25/255008.

(20) Martín-Jiménez, A.; Fernández-Domínguez, A. I.; Lauwaet, K.; Granados, D.; Miranda, R.; García-Vidal, F. J.; Otero, R. Unveiling the Radiative Local Density of Optical States of a Plasmonic Nanocavity by STM. *Nat. Commun.* **2020**, *11* (1), 1021. https://doi.org/10.1038/s41467-020-14827-7.

(21) Merino, P.; Rosławska, A.; Leon, C. C.; Grewal, A.; Große, C.; González, C.; Kuhnke, K.; Kern, K. A Single Hydrogen Molecule as an Intensity Chopper in an Electrically Driven Plasmonic Nanocavity. *Nano Lett.* **2019**, *19* (1), 235–241. https://doi.org/10.1021/acs.nanolett.8b03753.

(22) Leon, C. C.; Rosławska, A.; Grewal, A.; Gunnarsson, O.; Kuhnke, K.; Kern, K. Photon Superbunching from a Generic Tunnel Junction. *Sci. Adv.* **2019**, *5* (5), eaav4986. https://doi.org/10.1126/sciadv.aav4986.
(23) Kuhnke, K.; Große, C.; Merino, P.; Kern, K. Atomic-Scale Imaging and Spectroscopy of Electroluminescence at Molecular Interfaces. *Chem. Rev.* **2017**, *117* (7), 5174–5222. https://doi.org/10.1021/acs.chemrev.6b00645.
(24) Imada, H.; Miwa, K.; Jung, J.; Shimizu, T. K.; Yamamoto, N.; Kim, Y. Atomic-Scale Luminescence Measurement and Theoretical Analysis Unveiling Electron Energy Dissipation at a p -Type GaAs(110) Surface. *Nanotechnology* **2015**, *26* (36), 365402. https://doi.org/10.1088/0957-4484/26/36/365402.
(25) Mühlenberend, S.; Gruyters, M.; Berndt, R. Plasmon-Mediated Circularly Polarized Luminescence of GaAs in a Scanning Tunneling Microscope. *Appl. Phys. Lett.* **2015**, *107* (24), 241110. https://doi.org/10.1063/1.4938167.
(26) Doppagne, B.; Chong, M. C.; Bulou, H.; Boeglin, A.; Scheurer, F.; Schull, G. Electrofluorochromism at the Single-Molecule Level. *Science* **2018**, *361* (6399), 251–255. https://doi.org/10.1126/science.aat1603.
(27) Kimura, K.; Miwa, K.; Imada, H.; Imai-Imada, M.; Kawahara, S.; Takeya, J.; Kawai, M.; Galperin, M.; Kim, Y. Selective Triplet Exciton Formation in a Single Molecule. *Nature* **2019**, *570* (7760), 210. https://doi.org/10.1038/s41586-019-1284-2.
(28) Miwa, K.; Imada, H.; Imai-Imada, M.; Kimura, K.; Galperin, M.; Kim, Y. Many-Body State Description of Single-Molecule Electroluminescence Driven by a Scanning Tunneling Microscope. *Nano Lett.* **2019**, *19* (5), 2803–2811. https://doi.org/10.1021/acs.nanolett.8b04484.
(29) Zhang, Y.; Luo, Y.; Zhang, Y.; Yu, Y.-J.; Kuang, Y.-M.; Zhang, L.; Meng, Q.-S.; Luo, Y.; Yang, J.-L.; Dong, Z.-C.; Hou, J. G. Visualizing Coherent Intermolecular Dipole–Dipole Coupling in Real Space. *Nature* **2016**, *531* (7596), 623–627. https://doi.org/10.1038/nature17428.
(30) Imada, H.; Miwa, K.; Imai-Imada, M.; Kawahara, S.; Kimura, K.; Kim, Y. Real-Space Investigation of Energy Transfer in Heterogeneous Molecular Dimers. *Nature* **2016**, *538* (7625), 364–367. https://doi.org/10.1038/nature19765.
(31) Simmons, J. G. Generalized Formula for the Electric Tunnel Effect between Similar Electrodes Separated by a Thin Insulating Film. *J. Appl. Phys.* **1963**, *34* (6), 1793–1803. https://doi.org/10.1063/1.1702682.
(32) Kazuma, E.; Jung, J.; Ueba, H.; Trenary, M.; Kim, Y. Real-Space and Real-Time Observation of a Plasmon-Induced Chemical Reaction of a Single Molecule. *Science* **2018**, *360* (6388), 521–526. https://doi.org/10.1126/science.aao0872.
(33) Aragonès, A. C.; Haworth, N. L.; Darwish, N.; Ciampi, S.; Bloomfield, N. J.; Wallace, G. G.; Diez-Perez, I.; Coote, M. L. Electrostatic Catalysis of a Diels–Alder Reaction. *Nature* **2016**, *531* (7592), 88–91. https://doi.org/10.1038/nature16989.
(34) Lin, C. L.; Lu, S. M.; Su, W. B.; Shih, H. T.; Wu, B. F.; Yao, Y. D.; Chang, C. S.; Tsong, T. T. Manifestation of Work Function Difference in High Order Gundlach Oscillation. *Phys. Rev. Lett.* **2007**, *99* (21), 216103. https://doi.org/10.1103/PhysRevLett.99.216103.
(35) Zhang, R.; Zhang, Y.; Dong, Z. C.; Jiang, S.; Zhang, C.; Chen, L. G.; Zhang, L.; Liao, Y.; Aizpurua, J.; Luo, Y.; Yang, J. L.; Hou, J. G. Chemical Mapping of a Single Molecule by Plasmon-Enhanced Raman Scattering. *Nature* **2013**, *498* (7452), 82–86. https://doi.org/10.1038/nature12151.
(36) Lee, J.; Crampton, K. T.; Tallarida, N.; Apkarian, V. A. Visualizing Vibrational Normal Modes of a Single Molecule with Atomically Confined Light. *Nature* **2019**, *568* (7750), 78. https://doi.org/10.1038/s41586-019-1059-9.
(37) Jaculbia, R. B.; Imada, H.; Miwa, K.; Iwasa, T.; Takenaka, M.; Yang, B.; Kazuma, E.; Hayazawa, N.; Taketsugu, T.; Kim, Y. Single-Molecule Resonance Raman Effect in a Plasmonic Nanocavity. *Nat. Nanotechnol.* **2020**, *15* (2), 105–110. https://doi.org/10.1038/s41565-019-0614-8.
(38) Sanari, Y.; Tachizaki, T.; Saito, Y.; Makino, K.; Fons, P.; Kolobov, A. V.; Tominaga, J.; Tanaka, K.; Kanemitsu, Y.; Hase, M.; Hirori, H. Zener Tunneling Breakdown in Phase-Change Materials Revealed by Intense Terahertz Pulses. *Phys. Rev. Lett.* **2018**, *121* (16), 165702. https://doi.org/10.1103/PhysRevLett.121.165702.

Supporting Information

Terahertz-field-driven scanning tunneling luminescence spectroscopy

Kensuke Kimura[†], *Yuta Morinaga*[‡], *Hiroshi Imada*[*,†,§], *Ikufumi Katayama*[*,‡], *Kanta Asakawa*[‡], *Katsumasa Yoshioka*[‡,‖], *Yousoo Kim*[*,†], *Jun Takeda*[*,†,‡]

[†] Surface and Interface Science Laboratory, RIKEN, Wako, Japan.

[‡] Department of Physics, Graduate School of Engineering Science, Yokohama National University, Yokohama, Japan.

[§] PRESTO, Japan Science and Technology Agency (JST), Kawaguchi, Japan.

[‖] Present address: NTT Basic Research Laboratories, NTT Corporation, Atsugi, Japan.

*Correspondence to: himada@riken.jp (H.I.), katayama-ikufumi-bm@ynu.ac.jp (I.K.), ykim@riken.jp (Y.K.), or jun@ynu.ac.jp (J.T.)

I. Methods

THz pulse generation

Figure S1a shows a schematic of the THz pulse generation. We used a Yb fiber laser with a repetition rate of 100 kHz, pulse duration of 200 fs, center wavelength of 1030 nm, and the pulse energy of 8 μJ (FCPA μJewel, IMRA America Inc.). The 8 μJ laser pulse with relatively low repatriation rate allows us to implement the plasmon excitation with an extremely high transient voltage (~6.5 V) at an STM junction, as explained in sections II and III. Single-cycle THz pulses were generated using a $LiNbO_3$ prism with tilted pulse-front configuration[1–7]. The generated THz pulses were then collimated by an off-axis parabolic mirror and passed through a pair of wire grid polarizers (WGP#1 and #2) to tune the field strength. WGP#2 was fixed to introduce parallel-polarized THz pulses to the tip-sample direction, and the angle of WGP#1 with respect to WGP#2 was changed to control the electric field intensity, with the relative angle between the WGPs defined as θ.

The waveform and electric field strength of the generated THz pulses were evaluated by electro-optical (EO) sampling. The probe pulses for EO sampling were made collinear to the THz pulses by using a THz-near-infrared beam splitter and focusing onto an EO crystal (1 mm thick ZnTe(110) crystal). The electric field strength was evaluated by assuming an EO coefficient of r_{41} = 4.45 pm/V and refractive indices of $n_{1030\text{nm}} = 2.76$ and $n_{\text{THz}} = 3.17$. According to the EO sampling, the maximum field strength was 188 V/cm (Fig. 1b).

After the EO sampling, THz and probe pulses were guided into the STM by inserting a removable mirror. The probe pulse was used for optical alignment to couple the THz pulses with the STM tip. After the alignment, the probe pulse was blocked. During the STM experiments, a removable Si wafer was inserted into the path of the THz pulse to block undesired photons originating from sum-frequency generation (~515 nm) in $LiNbO_3$.

Coupling THz pulses with an STM

Figure S1b shows a schematic of the STM (Omicron) setup operating at 5.0 K under ultrahigh vacuum (UHV). For introducing the THz pulses into the STM, we used *z*-cut quartz as a view port and Tsurupica (Pax Co.) as optical windows attached to the radiation shields. The THz pulses were focused at the STM junction using an aspheric Tsurupica lens (11 mm diameter, 16.8 mm focal length). The small diameter of the lens enabled it to be mounted on the vibration-isolated stage of the low-temperature STM.

Figure S1c shows a typical current trace recorded with illuminating THz pulses. The drift in the tunnel current was sufficiently low (typically 0.05 pA/min) to ensure highly stable THz-STL measurements. Steady-state STL measurements were also conducted with the feedback loop turned off. Therefore, it was possible to compare the THz-STL and steady-state STL spectra (Fig.

3).

THz-STL and steady-state STL measurement

The emitted photons were collected using another glass achromatic lens (11 mm diameter, 17.5 mm focal length) and were directed out of the UHV chamber, where they were refocused onto a grating spectrometer (HRS-300, Princeton Instruments) equipped with a charge-coupled-device photon detector (PyLoN: 100BR eXcelon, Princeton Instruments) cooled with liquid nitrogen. In all the experiments, a grating with 50 grooves mm^{-1} was used.

To block undesired photons originating from the fundamental laser pulses and second-harmonics at the $LiNbO_3$ prism, 550 nm long-pass and 975 nm short-pass filters were placed in front of the spectrometer.

Preparation of sample and tip

A clean Ag(111) surface was prepared by repeated cycles of Ar^+ ion sputtering and annealing. Deposition of Au onto Ag(111) was performed using a home-made evaporator. The Ag(111) was kept at room temperature during the deposition. The STM tip was prepared by electrochemically etching a gold wire in KCl electrolyte[8]. Plasmon resonance of the tip was tuned by controlled-indentation and a voltage pulse on the Ag(111) surface, as we reported previously[9,10].

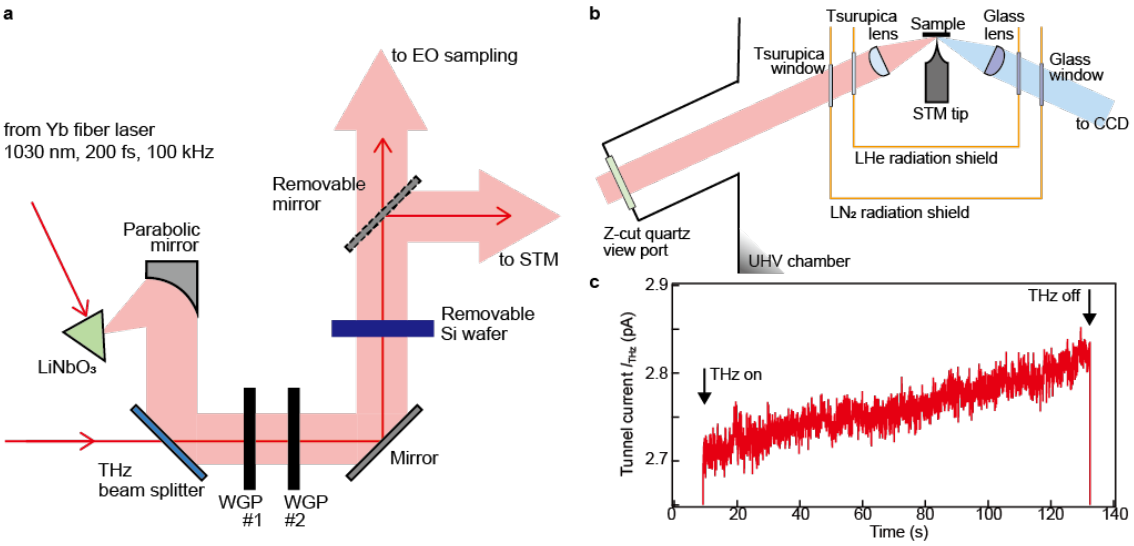

Figure S1 | Experimental details of THz-STL spectroscopy
(a) Schematic of THz generation. (b) Schematic of the STM setup. (c) Current trace with irradiating THz pulses (V_{DC} = 0 V).

II. Model calculation based on the Simmons model

By coupling the THz pulses to an STM tip, the electric field of THz (E_{THz}) was confined in the nanometer scale, and therefore enhanced at the junction[2–6,11–15]. Here, we evaluate the maximum value of V_{THz} in our setup using the I_{DC}-V_{DC} curve (Fig. S2a) and temporal profile of the THz pulse (Fig. 1b). The measured value of I_{THz} (e.g. I_{THz} = 2.65 pA in Fig. 1c) is the summation of the temporal current variation because the response of the STM electronics is much slower than the picosecond THz transients. As shown in Fig. S2a, a positive V_{THz} gives a positive current (red area), whereas a negative V_{THz} gives a negative current (blue area). Therefore, the measured I_{THz} is given by

$$I_{\mathrm{THz}} = \int I_{\mathrm{THz}}(t)\,\mathrm{d}t = \int I_{\mathrm{DC}}(V_{\mathrm{THz}}(t))\,\mathrm{d}t. \qquad (1)$$

This equation can be used to evaluate the maximum value of V_{THz} as follows[11].

The current generated by a THz pulse can be roughly estimated as tens of μA by considering the current trace result of I_{THz} = 2.65 pA (Fig. 1c) and repetition rate of 100 kHz. Therefore, it is not possible to just use the experimentally obtained I_{DC}-V_{DC} curve (Fig. S2a) to evaluate the maximum value of V_{THz}. To extrapolate the I_{DC}-V_{DC} curve over tens of μA, we assumed that the I_{DC}-V_{DC} characteristics followed the Simmons model[13], which has been utilized in previous THz-STM studies[4,5,11]. We used the following equation for the Simmons model in the field emission region:

$$J = \frac{2.2e^3F^2}{8\pi h\phi}\left\{\exp\left[-\frac{8\pi}{2.96heF}(2m)^{\frac{1}{2}}\phi^{\frac{3}{2}}\right]\right.$$
$$\left.-\left(1+\frac{2eV_{\mathrm{DC}}}{\phi}\right)\exp\left[-\frac{8\pi}{2.96heF}(2m)^{\frac{1}{2}}\phi^{\frac{3}{2}}\left(1+\frac{2eV_{\mathrm{DC}}}{\phi}\right)^{\frac{1}{2}}\right]\right\} \qquad (2)$$

where J is the current density, e is the elementally charge, h is the Planck constant, m is the mass of an electron, s is the tunnel barrier width and ϕ is the effective work function. F indicates the strength of the field given by $F = V_{\mathrm{DC}}/s$. Figure S2b shows the extrapolated I_{DC}-V_{DC} curve based on the Simmons model. By using this extrapolated I_{DC}-V_{DC} curve and the THz temporal profile (Fig. 1b), we calculated I_{THz} from equation (1) and evaluated the maximum value of V_{THz} as ~6.5 V. Figure S2c shows temporal profile of THz-induced tunneling current ($I_{THz}(t)$). According to the simulation, the most of tunneling electrons flow at around 3.5 ps, where V_{THz} reaches ~6.5 V (I = ~250 μA)[14]. Furthermore, the THz intensity dependence of I_{THz} (Fig. 2b) was reasonably well reproduced (Fig. S2c), supporting our model calculation using the far-field THz wave form[5,6].

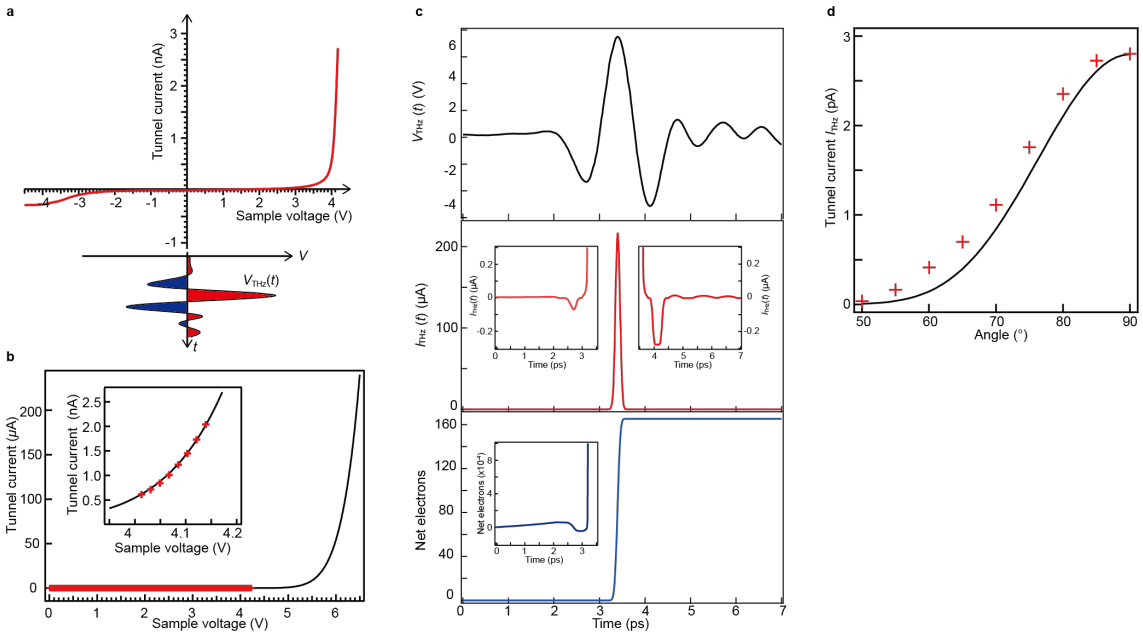

Figure S2 | Estimation of V_{THz} based on the Simmons model

(a) Experimentally obtained I_{DC}-V_{DC} spectrum of Ag(111) (red line in upper panel). The feedback loop was turned off at V_{DC} = 1.0 V, I_{DC} = 10 pA. The lower panel shows a schematic of the temporal tunnel current induced by a THz pulse. The red area indicates a positive current, whereas the blue area indicates a negative current. (b) Extrapolated I_{DC}-V_{DC} curve based on the Simmons model. Red cross points show the experimental results (identical with Fig. S2a) and the black line shows the calculation result. The inset shows a magnification of the curve at around 4 V (field emission region). (c) Temporal profile of THz pulse (upper row), simulation of $I_{THz}(t)$ (middle row), and simulation of the number of net transported electron (lower row). The inset figures magnify at V_{THz} < ~4 V region. (d) Dependence of I_{THz} on the relative angle (θ) between the wire grid polarizers. Red cross points show the experimental results, whereas the black line shows the simulated results.

III. Comparison of plasmon excitation efficiency between field- and DC-driven electrons

For comparison of the plasmon excitation efficiency of field- and DC-driven electrons, we conducted THz-STL and steady-state STL measurements without changing the distance between the tip and metal surface (constant height mode). The grey spectrum in Fig. S3a shows the steady-state STL spectrum with the feedback loop turned off at V_{DC} = 2.5 V and I_{DC} = 10 pA, whereas the red spectrum is the THz-STL spectrum. By adjusting V_{DC} = 3.14 V, the tunnel current in the steady-state STL measurement became the same value as that in the THz-STL measurement, as shown in the inset. The blue spectrum was obtained under this condition. The luminescence intensity of the blue spectrum is larger than that of the red spectrum, indicating that the plasmon excitation efficiency of I_{THz} was smaller than that of I_{DC}. The subtracted spectra are shown in Fig. S3b and S3c, which show that the plasmon excitation efficiency by the field-driven electrons was 10 times smaller than by the DC-driven electrons. By correcting the detection efficiency of our setup, the electron-photon conversion efficiencies of THz-STL and STL in Fig. 3a were calculated as 0.012% and 0.095%, respectively.

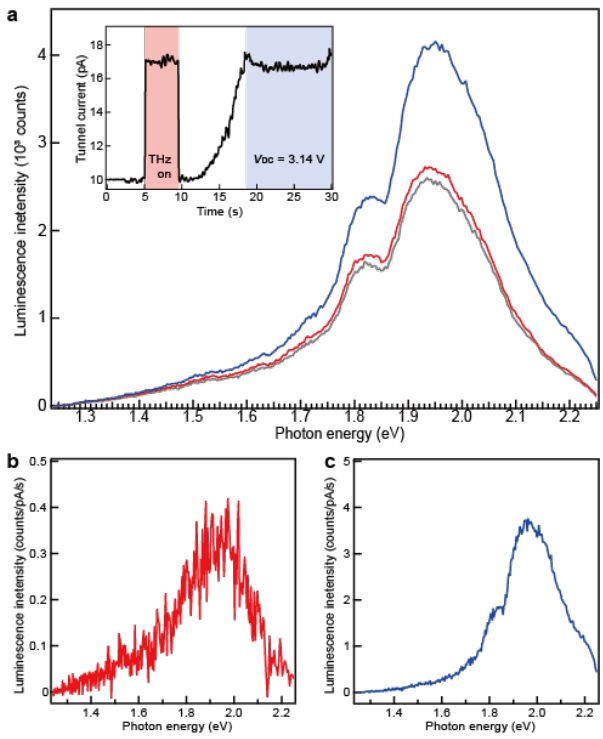

Figure S3 | Comparison of plasmon excitation efficiencies between I_{THz} and I_{DC}
(a) THz-STL spectrum and STL spectra with the feedback loop turned off at V_{DC} = 2.5 V and I_{DC} = 10 pA. The grey spectrum was obtained under the aforementioned conditions, whereas the red spectrum was obtained with further illuminating THz pulses. The blue spectrum was obtained at V_{DC} = 3.14 V while keeping the tip height constant. The inset shows the current trace in this measurement. (b) Subtraction of grey spectrum from red spectrum in Fig. S3a. (c) Subtraction of grey spectrum from blue spectrum in Fig. S3a.

To elucidate the origin of the efficiency difference between field- and DC-driven electrons, we considered that V_{THz} varied within the picosecond timescale and reached a maximum of ~6.5 V (Fig. S2), where the experimental conditions included the field emission (FE) region as well as the tunneling region. Figure S4a shows a dZ-dV_{DC} spectrum of Ag(111) obtained by measuring the distance between the STM tip and metal surface (Z) as a function of V_{DC}. Multiple peaks in the dZ-dV_{DC} spectrum corresponded to resonant tunneling through the FE resonances (FERs) of the STM junction.

The luminescence from a localized plasmon at V_{DC} in the FE region was previously studied by the steady-state STL at constant current mode[16,17]. They found that the efficiency changes in accordance with V_{DC}, as schematically shown in Fig. S4b-d. When V_{DC} is in the tunneling region, inelastically tunneled electrons excite the localized plasmon (Fig. S4b). When V_{DC} is set at the voltage of the 1st FER peak (V_{1st}), elastic tunneling to the FER becomes the dominant tunneling channel (Fig. S4c). Since the localized plasmon is excited via the inelastic tunneling (IET) process, the luminescence efficiency is small at around V_{1st}. When the voltage is increased to $V_{1st} + h\nu/e$, IET pathways via the 1st FER, which accompanies the plasmon excitation, are opened (Fig. S4d), resulting in increased luminescence efficiency.

In the previous studies[16,17], steady-state STL measurements were conducted with the constant current mode. Since the tip height was kept constant in our THz-STL measurements, we confirmed an efficiency decrease at around V_{1st} with the constant height mode. Figure S5a shows three steady-state STL spectra obtained at V_{DC} = 3.0 V (tunneling region), 4.0 V (the 1st FER peak position, V_{1st}) and 4.5 V (above the 1st FER peak position). The red spectrum in Fig. S5a is the STL spectrum obtained at V_{DC} = 3.0 V and I_{DC} = 10 pA. When V_{DC} was changed to 4.0 V with the feedback turned off, the current increased to ~170 pA (blue line in Fig. S5b) and the luminescence intensity also increased (blue spectrum in Fig. S5a). Similarly, when V_{DC} was changed to 4.5 V, the current increased to ~13 nA (purple line in Fig. S5b) and the intensity also increased (purple spectrum in Fig. S5a). Figure S5c shows the efficiencies of the plasmon luminescence at V_{DC} = 3.0, 4.0 and 4.5 V, clearly indicating that the efficiency was reduced at around V_{1st} (Fig. S4c). Because of the limitations of our STM's current amplifier, we could not confirm whether the efficiency recovered at $V_{1st} + h\nu/e$ in the constant height mode. However, it can be expected that the efficiency would substantially recover since there is no tip retraction in the case of constant height mode (Fig. S4d).

The voltage dependence of the efficiency in steady-state STL spectroscopy may also be applicable to THz-STL spectroscopy because $V_{THz}(t)$ can be treated as quasi-static for the plasmon owing to its femtosecond lifetime[14]. On the basis of all the results and discussions, we concluded that the luminescence efficiency during THz-STL measurement varied within the picosecond timescale owing to the time evolution of $V_{THz}(t)$ (Fig. 4), which was responsible for the efficiency

difference observed in Figs. 3 and S3.

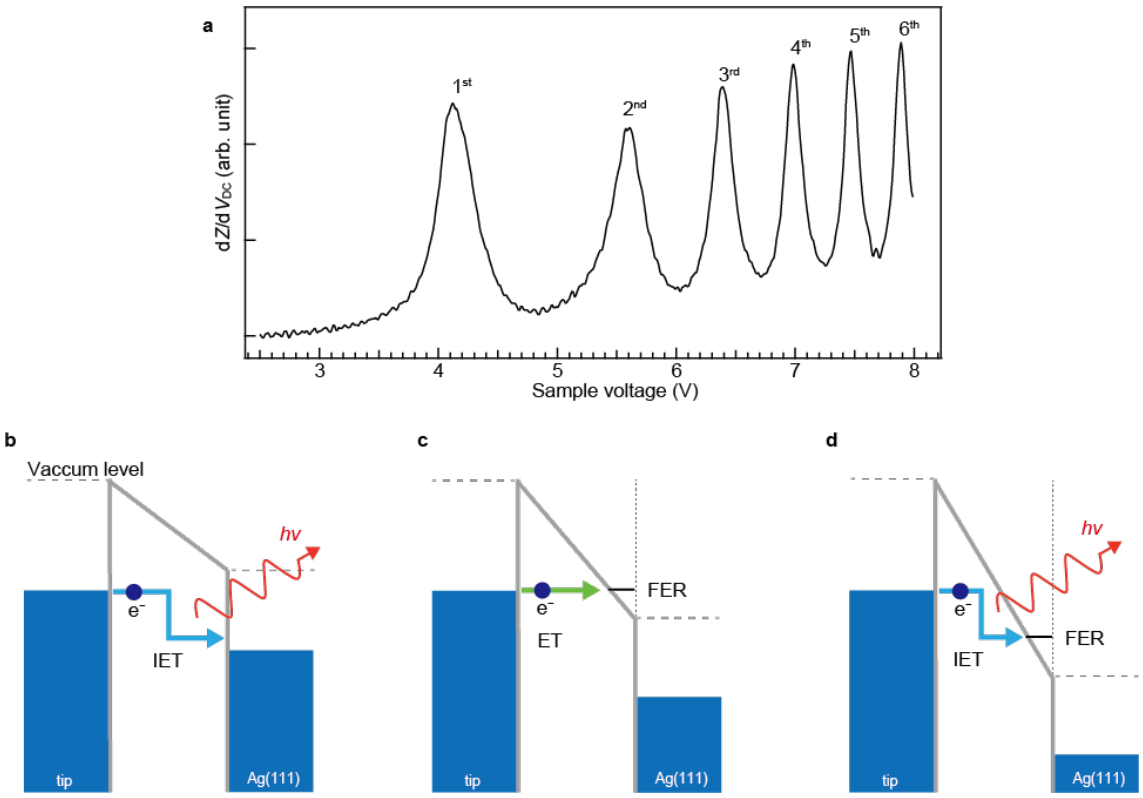

Figure S4 | Energy diagrams in the tunnel and field emission regions

(a) dZ/dV_{DC} spectrum of Ag(111) (I_{DC} = 10 pA). Multiple peaks in the spectrum (labelled as 1st, 2nd …) originate from the FERs. (b-d) Schematic energy diagrams. Blue rectangles indicate the density of states of the tip and Ag(111). (b) V_{DC} is at the tunnelling region, (c) V_{DC} is around V_{1st}, (d) V_{DC} is around V_{1st} + $h\nu/e$. Elastic tunnelling to the 1st FER is dominant in (c), which causes a decrease in luminescence efficiency, as observed in Fig. S5.

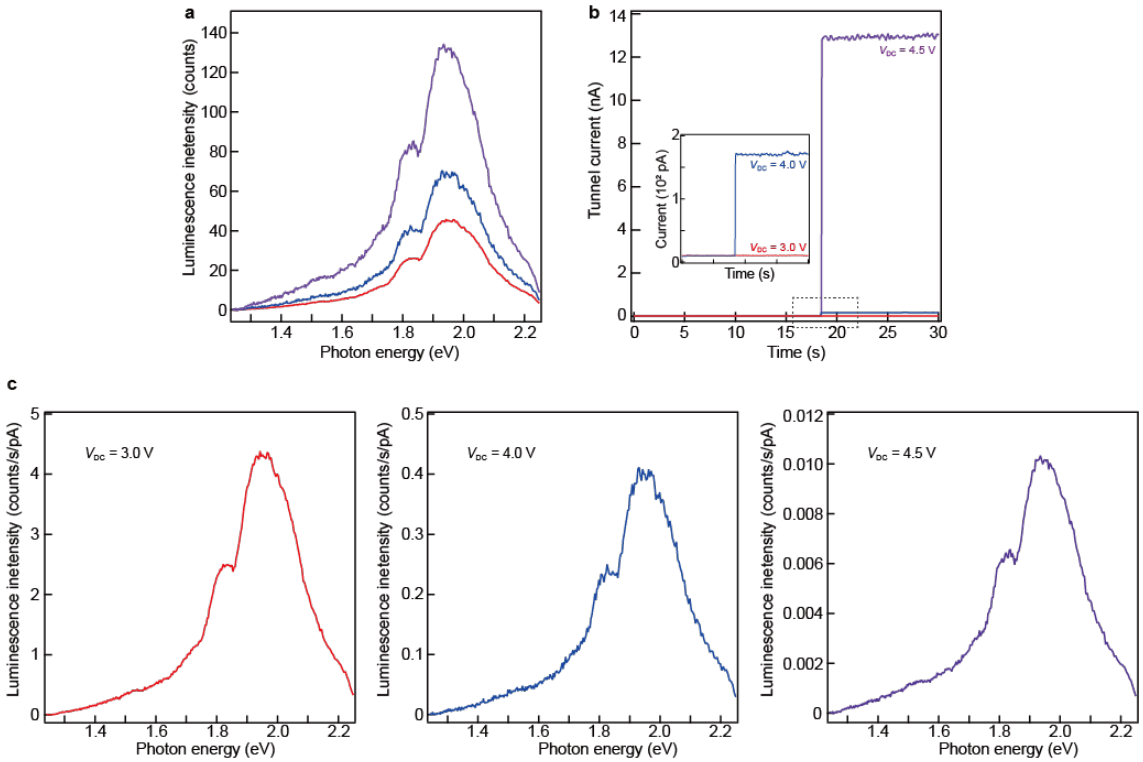

Figure S5 | Efficiency of plasmon luminescence in the field emission region

(a) Three STL spectra at V_{DC} = 3.0 (red), 4.0 (blue) and 4.5 V (purple). The feedback loop was turned off at V_{DC} = 3.0 V and I_{DC} = 10 pA in all measurements. (b) Three current traces at V_{DC} = 3.0 (red), 4.0 (blue) and 4.5 V (purple). The inset magnifies the grey rectangular region of the main panel. (c) Three STL (efficiency) spectra at V_{DC} = 3.0 (red, left panel), 4.0 (blue, centre panel) and 4.5 V (purple, right panel). The spectra in Fig. S5(a) were divided by the I_{DC} in Fig. S5(b).

References

(1) Hebling, J.; Almási, G.; Kozma, I. Z.; Kuhl, J. Velocity Matching by Pulse Front Tilting for Large-Area THz-Pulse Generation. *Opt. Express* **2002**, *10* (21), 1161–1166. https://doi.org/10.1364/OE.10.001161.

(2) Peller, D.; Kastner, L. Z.; Buchner, T.; Roelcke, C.; Albrecht, F.; Moll, N.; Huber, R.; Repp, J. Sub-Cycle Atomic-Scale Forces Coherently Control a Single-Molecule Switch. *Nature* **2020**, *585* (7823), 58–62. https://doi.org/10.1038/s41586-020-2620-2.

(3) Cocker, T. L.; Peller, D.; Yu, P.; Repp, J.; Huber, R. Tracking the Ultrafast Motion of a Single Molecule by Femtosecond Orbital Imaging. *Nature* **2016**, *539* (7628), 263–267. https://doi.org/10.1038/nature19816.

(4) Yoshioka, K.; Katayama, I.; Minami, Y.; Kitajima, M.; Yoshida, S.; Shigekawa, H.; Takeda, J. Real-Space Coherent Manipulation of Electrons in a Single Tunnel Junction by Single-Cycle Terahertz Electric Fields. *Nat. Photonics* **2016**, *10* (12), 762–765. https://doi.org/10.1038/nphoton.2016.205.

(5) Yoshioka, K.; Katayama, I.; Arashida, Y.; Ban, A.; Kawada, Y.; Konishi, K.; Takahashi, H.; Takeda, J. Tailoring Single-Cycle Near Field in a Tunnel Junction with Carrier-Envelope Phase-Controlled Terahertz Electric Fields. *Nano Lett.* **2018**, *18* (8), 5198–5204. https://doi.org/10.1021/acs.nanolett.8b02161.

(6) Yoshida, S.; Hirori, H.; Tachizaki, T.; Yoshioka, K.; Arashida, Y.; Wang, Z.-H.; Sanari, Y.; Takeuchi, O.; Kanemitsu, Y.; Shigekawa, H. Subcycle Transient Scanning Tunneling Spectroscopy with Visualization of Enhanced Terahertz Near Field. *ACS Photonics* **2019**, *6* (6), 1356–1364. https://doi.org/10.1021/acsphotonics.9b00266.

(7) Hirori, H.; Doi, A.; Blanchard, F.; Tanaka, K. Single-Cycle Terahertz Pulses with Amplitudes Exceeding 1 MV/Cm Generated by Optical Rectification in LiNbO3. *Appl. Phys. Lett.* **2011**, *98* (9), 091106. https://doi.org/10.1063/1.3560062.

(8) Yang, B.; Kazuma, E.; Yokota, Y.; Kim, Y. Fabrication of Sharp Gold Tips by Three-Electrode Electrochemical Etching with High Controllability and Reproducibility. *J. Phys. Chem. C* **2018**, *122* (29), 16950–16955. https://doi.org/10.1021/acs.jpcc.8b04078.

(9) Imada, H.; Miwa, K.; Imai-Imada, M.; Kawahara, S.; Kimura, K.; Kim, Y. Single-Molecule Investigation of Energy Dynamics in a Coupled Plasmon-Exciton System. *Phys. Rev. Lett.* **2017**, *119* (1), 013901. https://doi.org/10.1103/PhysRevLett.119.013901.

(10) Kimura, K.; Miwa, K.; Imada, H.; Imai-Imada, M.; Kawahara, S.; Takeya, J.; Kawai, M.; Galperin, M.; Kim, Y. Selective Triplet Exciton Formation in a Single Molecule. *Nature* **2019**, *570* (7760), 210. https://doi.org/10.1038/s41586-019-1284-2.

(11) Cocker, T. L.; Jelic, V.; Gupta, M.; Molesky, S. J.; Burgess, J. A. J.; Reyes, G. D. L.; Titova, L. V.; Tsui, Y. Y.; Freeman, M. R.; Hegmann, F. A. An Ultrafast Terahertz Scanning

Tunnelling Microscope. *Nat. Photonics* **2013**, *7* (8), 620–625. https://doi.org/10.1038/nphoton.2013.151.

(12) Jelic, V.; Iwaszczuk, K.; Nguyen, P. H.; Rathje, C.; Hornig, G. J.; Sharum, H. M.; Hoffman, J. R.; Freeman, M. R.; Hegmann, F. A. Ultrafast Terahertz Control of Extreme Tunnel Currents through Single Atoms on a Silicon Surface. *Nat. Phys.* **2017**, *13*, 591–598. https://doi.org/10.1038/nphys4047.

(13) Müller, M.; Martín Sabanés, N.; Kampfrath, T.; Wolf, M. Phase-Resolved Detection of Ultrabroadband THz Pulses inside a Scanning Tunneling Microscope Junction. *ACS Photonics* **2020**, *7* (8), 2046–2055. https://doi.org/10.1021/acsphotonics.0c00386.

(14) Luo, Y.; Jelic, V.; Chen, G.; Nguyen, P. H.; Liu, Y.-J. R.; Calzada, J. A. M.; Mildenberger, D. J.; Hegmann, F. A. Nanoscale Terahertz STM Imaging of a Metal Surface. *Phys. Rev. B* **2020**, 102 (20), 205417. https://doi.org/10.1103/PhysRevB.102.205417.

(15) Garg, M.; Kern, K. Attosecond Coherent Manipulation of Electrons in Tunneling Microscopy. *Science* **2020**, *367* (6476), 411–415. https://doi.org/10.1126/science.aaz1098.

(16) Berndt, R.; Gimzewski, J. K. Isochromat Spectroscopy of Photons Emitted from Metal Surfaces in an STM. *Ann. Phys.* **1993**, *505* (2), 133–140. https://doi.org/10.1002/andp.19935050205.

(17) Martínez-Blanco, J.; Fölsch, S. Light Emission from Ag(111) Driven by Inelastic Tunneling in the Field Emission Regime. *J. Phys. Condens. Matter* **2015**, 27 (25), 255008. https://doi.org/10.1088/0953-8984/27/25/255008.